

Article

Deterministic Prediction of the Entropy Increase in a Sudden Expansion

LaVar King Isaacson

Professor Emeritus of Mechanical Engineering, University of Utah, 2067 Browning Avenue, Salt Lake City, UT 84108, USA; E-Mail: lkisaacson1@mac.com

Received: 24 December 2010; in revised form: 25 January 2011 / Accepted: 25 January 2011 /

Published: 31 January 2011

Abstract: This paper presents the results of a study of the prediction of the entropy growth within an internal free shear layer of an ideal gas flow downstream of a sudden expansion of the flow area. The objective of the study is exploratory in nature by invoking concepts from information theory to connect the deterministic prediction of the spectral entropy growth within the shear layer to the experimentally inferred increase in entropy across the flow region. The deterministic prediction of the spectral entropy increase along the shear layer is brought into agreement with the experimentally inferred increase in entropy through the *ad hoc* inclusion of the activation spectral entropy. The values for this activation spectral entropy are directly related to the area ratios across the expansion region and have a specific numerical value for each area ratio.

Keywords: experimental stagnation pressure losses; deterministic flow equations; spectral entropy predictions

PACS Codes: 05.45.Pq (Numerical simulation of chaotic systems), 05.70.Ln (Nonequilibrium thermodynamics and irreversible thermodynamics), 47.15.St (Free shear layers), 47.20.Ky (Instability of shear layers), 89.70.Cf (Entropy and other measures of information)

Nomenclature:

a_i	Fluctuating i-th component of velocity wave vector
A_0	Upstream duct area
A_1	Initial duct area into expansion
A_2	Downstream duct area
f_r	Sum of the squares of the fluctuating vertical and transverse velocity wave vectors
F_1	Time-dependent perturbation factor
h_t	Stagnation enthalpy of the flow
k	Fluctuating wave number of Fourier expansion
K_1	Adjustable weight factor
M_1	Mach number of the flow at area A_1
p	Hydrostatic pressure
P_r	Power spectral density of the r-th spectral peak
P_t	Stagnation pressure of the flow
P_{t1}	Stagnation pressure at area A_1
P_{t2}	Stagnation pressure at area A_2
R	Appropriate gas constant
s	Specific entropy of the flow
s_1	Specific entropy at area A_1
s_2	Specific entropy at area A_2
s_{2_act}	Activation spectral entropy
s_{j_spent}	Spectral entropy for the j-th time series data segment
s_{1_spent}	Average of the spectral entropies over the entire time series
s_{2_spent}	Average of the spectral entropies above the activation spectral entropy
$\Delta S_{\text{exprmtl}}$	Experimental entropy change across the expansion
ΔS_{spent}	Spectral entropy change across the expansion
t	Time
T_t	Stagnation temperature of the flow
u_i	Fluctuating i-component of velocity
U_i	Mean velocity in the i-direction
v_t	Stagnation specific volume of the flow
V_y	Mean vertical velocity in the x-y plane
V_z	Mean vertical velocity in the y-z plane
W	Mean velocity in the span wise direction
x	Axial direction
x_i	i-th direction
x_j	j-th direction
y	Vertical direction
z	Span wise direction

Greek Letters

δ_{lm}	Kronecker delta
γ	Ratio of specific heats
ν	Kinematic viscosity

Subscripts

i, j, l, m	Tensor indices
r	The r -th index in the j -th time series data segment
t	Stagnation state
x	Component in the x-direction
y	Component in the y-direction
z	Component in the z-direction
1	Initial state at area A_1
2	Final state at area A_2

1. Introduction

The engineering evaluation of the flow of an ideal gas downstream of a sudden expansion or backward-facing step is a highly developed field in computational fluid dynamics (Gosman *et al.* [1], Patankar [2–3], Hirsch [4]). Abu-Nada [5] and Yapici *et al.* [6] have published recent articles that provide both extensive results for the entropy developed in such flows and references to work in this field.

Our objective here is to use this well-studied environment as a tool to test the hypothesis arising from information theory that the spectral entropy predicted from the solution of the time-dependent fluctuation form of the shear layer equations may be connected to the actual entropy increase observed across the flow region downstream of a sudden expansion.

We use as a basis for this study an observation from information theory (Jaynes [7]). We consider the experimental results for the loss of stagnation pressure across a dump combustor as measured by Barclay [8], and correlated by Oates [9] as the benchmark against which we are going to compare our theoretical predictions. In this study, we will consider the flow medium to be air. To model our predictions, we consider the internal free shear layer following the separation of the flow from the edge of the sudden expansion into the expansion volume. We model the three continuity equations and the three equations of motion for the fluctuating velocity components along the shear flow. We include the physics appropriate for an internal free shear layer, including the nonlinear coupling terms between the velocity components within the equations of motion.

From the computational results, we calculate the spectral entropy for the square of the fluctuating vertical and transverse velocity components along the shear layer as a function of time step. We then explore additional assumptions that must be made to bring the predicted spectral entropy increase in line with the entropy increase implied by the measured loss of stagnation pressure across the dump combustor. We find that an internal feedback coefficient must be included that is of a form found in the perturbation theory of quantum theory and must be of small magnitude. We also find that the

activation spectral entropy must be introduced to allow the numerical value of the predicted spectral entropy increase to match the experimental value. These results lead to the observation that the generation of spectral entropy in the flow into a sudden expansion may be of the transition rate theory type, with the transition as a type of dissolution of previously ordered flow structures, transferring information into entropy generated by irreversible processes.

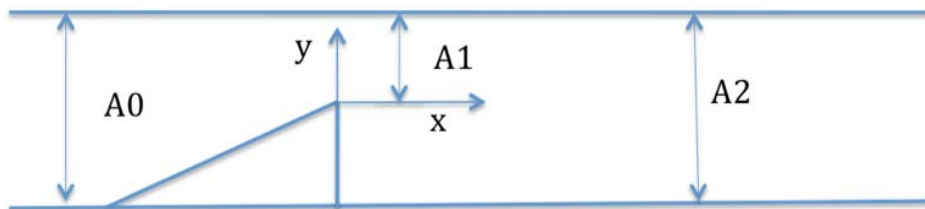
2. Mathematical Model for the Internal Free Shear Layer

The basic objective of this study is to attempt to bring the predictions from the solution of deterministic equations for the entropy increase of an ideal gas through a sudden expansion into agreement with the experimentally inferred increase in entropy for such a flow configuration. This configuration is chosen to model the experimental flow environment.

2.1. Mathematical Model

The flow configuration we wish to model is the three-dimensional internal free shear layer downstream of the separation point from the beginning of the sudden expansion at area A_1 , as indicated in Figure 1. The flow is from left to right and is assumed to be an ideal gas moving at subsonic velocity throughout the expansion from area A_1 to area A_2 .

Figure 1. The three-dimensional flow model and the coordinate system for the sudden expansion representing both the experimental environment and the mathematical model. The z -direction is normal to the x - y plane.



The Navier-Stokes equations describing this flow are transformed through a Fourier analysis into a Lorenz-type format, specifically keeping the nonlinear coupling terms. The coefficient of the nonlinear terms is simplified into a form obtained from the perturbation theory of non-relativistic quantum mechanics as described by Landau and Lifshitz [10]. Using the Fourier expansion procedure as presented by Townsend [11], the equations of motion for the internal free shear layer may be separated into steady plus fluctuating values of the velocity components. The velocity fluctuations around the mean values of the velocity components will thus be of primary interest, while the mean values of the velocity components will be obtained from assumed stream functions for the axial and span-wise flow parameters.

The equations for the velocity fluctuations may be written as follows [11]:

$$\frac{\partial u_i}{\partial t} + U_i \frac{\partial u_i}{\partial x_j} + u_i \frac{\partial U_i}{\partial x_j} + u_i \frac{\partial u_i}{\partial x_j} = -\frac{\partial p}{\partial x_i} + \nu \frac{\partial^2 u_i}{\partial x_j^2} \quad (1)$$

In these equations, ν is the kinematic viscosity. The pressure term may be transformed as:

$$-\frac{\partial^2 p}{\partial x_l^2} = 2 \frac{\partial U_l}{\partial x_m} \frac{\partial u_m}{\partial x_l} + \frac{\partial u_l}{\partial x_m} \frac{\partial u_m}{\partial x_l} \tag{2}$$

As Townsend [11] points out, the pressure is determined by the velocity and temperature fields and is not a local quantity but depends on the entire field of velocity and temperature. The elimination of the pressure fluctuation term introduces nonlinear coupling between the velocity coefficients. In our work here, we will introduce an internal feedback mechanism that will model the nonlinear interaction process but will allow the resulting equations to be integrated in time. Expanding the velocity fluctuations in terms of a sum of Fourier components:

$$u_i(x) = \sum a_i(k) \exp(ik \cdot x). \tag{3}$$

The variation with time of each Fourier component of the fluctuation field is then given by the equation for each of the velocity wave vector amplitudes:

$$\begin{aligned} \frac{da_i(k)}{dt} = & -\nu k^2 a_i(k) - \frac{\partial U_i}{\partial x_i} a_i(k) + 2 \frac{k_l k_l}{k^2} \frac{\partial U_l}{\partial x_m} a_i(k) \\ & + i \sum_{k'+k''=k} (k_l \frac{k_l k_m}{k^2} - \delta_{im} k_l) a_i(k') a_m(k''). \end{aligned} \tag{4}$$

The equations for the rate of change of the wave numbers are:

$$\frac{dk_i}{dt} = -\frac{\partial U_l}{\partial x_i} k_l. \tag{5}$$

The equations for the fluctuating velocity components may then be transformed by Fourier expansion into a form similar to Lorenz-type equations, as shown by Hellberg and Orszag [12] and Isaacson [13]. The equations resulting from the transformation process have been presented in other publications and references to them may be found in Isaacson [13].

At this point, we wish to introduce our first approximation to the set of first-order nonlinear differential equations describing the equations of motion of the fluctuating velocity components. We substitute the term $(1 - F_1)$ as the coefficient of the nonlinear terms in the equations for the time rate of change of the $a_i(k)$ coefficients. In this expression (Pyragas [14,15]):

$$F_1 = K_1 \cdot k(t). \tag{6}$$

where K_1 is the adjustable weight of the perturbation and $k(t)$ is the magnitude of the time-dependent wave vector given by:

$$k(t) = (k_x^2 + k_y^2 + k_z^2)^{1/2}. \tag{7}$$

The magnitude of the wave vector, $k(t)$, is computed at each time step in the integration process. The value for K_1 has been set to $5 \cdot 10^{-3}$ which allows the computations to remain stable throughout the time step range for each of the area ratios examined.

The three deterministic equations for the velocity coefficients may then be written as:

$$\begin{aligned} \frac{da_x}{dt} = & \left[\left(\frac{2k_x k_x}{k^2} - 1 \right) \frac{\partial U}{\partial y} + \frac{2k_x k_y}{k^2} \frac{\partial V_x}{\partial y} + \frac{2k_x k_z}{k^2} \frac{\partial W}{\partial y} \right] a_y \\ & - \left\{ \nu k^2 - \left[\left(\frac{2k_x k_x}{k^2} - 1 \right) \frac{\partial U}{\partial x} + \frac{2k_x k_y}{k^2} \frac{\partial V_x}{\partial x} + \frac{2k_x k_z}{k^2} \frac{\partial W}{\partial x} \right] \right\} a_x \end{aligned} \quad (8)$$

$$\begin{aligned} \frac{da_y}{dt} = & -(1 - F_1) a_x a_z + \left[\frac{2k_y k_x}{k^2} \frac{\partial U}{\partial x} + \left(\frac{2k_y k_y}{k^2} - 1 \right) \frac{\partial V_x}{\partial x} + \frac{2k_y k_z}{k^2} \frac{\partial W}{\partial x} \right] a_x \\ & - \left\{ \nu k^2 - \left[\frac{2k_y k_x}{k^2} \frac{\partial U}{\partial y} + \left(\frac{2k_y k_y}{k^2} - 1 \right) \frac{\partial V_x}{\partial y} + \frac{2k_y k_z}{k^2} \frac{\partial W}{\partial y} \right] \right\} a_y \end{aligned} \quad (9)$$

$$\frac{da_z}{dt} = (1 - F_1) a_x a_y - \left\{ \nu k^2 - \left[\frac{2k_z k_x}{k^2} \frac{\partial U}{\partial z} + \frac{2k_z k_y}{k^2} \frac{\partial V_x}{\partial z} + \left(\frac{2k_z k_z}{k^2} - 1 \right) \frac{\partial W}{\partial z} \right] \right\} a_z \quad (10)$$

Note that the perturbation factor $(1 - F_1)$ is applied to the nonlinear terms in the equations for $\frac{da_y}{dt}$ and $\frac{da_z}{dt}$, and not to one of the directly accessible dependent variables. This is a significant change from the practice in the study of synchronization and chaos (Pyragas [15]). The form of the perturbation factor and the application of the factor to the nonlinear terms are motivated by the perturbation analysis of the wave functions in non-relativistic quantum mechanics. This has been demonstrated by a specific example reported in Landau and Lifshitz [10]. The application of the perturbation factor in this fashion implies that the nonlinear terms in the first-order equations for the velocity fluctuations represent transition probabilities from an initial state to a secondary state. This observation is relevant to the inclusion of the *activated spectral entropy* concept in the interpretation of the final results (Glasstone, Laidler, and Eyring [16]).

The equations for the mean velocity gradients in the x-y and y-z planes of the shear layer are obtained from stream functions as used by Stuart [17] and Kirchoff [18] (see reference [13]). These relationships allow the gradients of the various mean velocities to be evaluated at specified locations within the shear layer.

The theoretical modeling of the internal free-shear layer consists of six simultaneous first-order differential equations, three linear equations accounting for continuity of mass and three non-linear, coupled equations describing the equations of motion. The numerical method includes computation of the velocity profiles, the mean velocity gradients, the thermodynamic and viscous properties of the fluid involved, with the solution yielding the velocity-fluctuation wave-vectors in three-dimensions for each of the imposed increases in area ratio, $\frac{A_2}{A_1}$, across the sudden expansion. From the conservation of mass from area A_1 to area A_2 , and assuming incompressible flow, the velocity ratio from the entrance to the exit of the expansion region, $\frac{U_1}{U_2}$, may be approximated as:

$$\frac{U_1}{U_2} = \frac{1}{\frac{A_1}{A_2}} \quad (11)$$

This relationship provides the initial conditions for the fluctuating velocity components for each set of area ratios reported in the experimental results:

$$a_x(0) = \frac{1}{\frac{A_1}{A_2}}; \quad a_y(0) = 0.0; \quad a_z(0) = 0.0. \quad (12)$$

The set of area ratios for the sudden expansion are:

$$\frac{A_1}{A_2} = \{0.90, 0.80, 0.70, 0.60, 0.50, 0.40, 0.30\}. \quad (13)$$

These values yield the initial fluctuating axial velocity ratios as:

$$a_x(0) = \{1.11, 1.25, 1.43, 1.67, 2.00, 2.50, 3.33\}. \quad (14)$$

The squares of these values represent the magnitude of the input fluctuating kinetic energy for each area ratio that is then available for dissolution into the final entropy values.

These equations are integrated using a fourth-order Runge-Kutta technique with source codes as presented by Press, *et al.* [19]. First, the three first-order differential equations for the wave numbers are integrated in time with the resulting series stored to files on the hard drive. A total of 24,576 time steps are included in the integration process. Then, the three first-order differential equations for the fluctuation velocity terms are solved, with the resulting time-series again stored in files. These data files thus become available for the spectral analysis as described in the next section.

2.2. The Prediction of Spectral Entropy from the Deterministic Results

There are a number of methods of analysis that may be used to predict the spectral entropy from the nonlinear time series results of the deterministic computations. Several that may be mentioned include the method of Singular Spectrum Analysis (SSA), the Principal Component Analysis (PCA) and the Maximum Entropy Method (MEM).

The method of Singular Spectrum Analysis (SSA) is well described by Golyandina *et al.* [20], and, as an example, applied to the forecasting of industrial production in several European economies by Hassani *et al.* [21]. Singular value decomposition (SVD) techniques are used extensively in the SSA method, with a series of useful computer source codes given in Press *et al.* [22].

Kantz and Schreiber [23] describe the Principal Component Analysis (CPA) method for the analysis of nonlinear time series data. These investigators have developed a package of computer software with the general title “Nonlinear Time Series Analysis”, as a publicly available computer package under the name TISEAN.

Maindonald and Braun [24] present an example-based approach to the use of the R computing environment for a statistical methodology that emphasizes the use of graphical presentations. It is designed for use by investigators who wish to do statistical analyses on their own data. This computing environment is publicly available through the Comprehensive R Archive Network (CRAN).

Finally, the Maximum Entropy Method (MEM) (Press *et al.* [25]) is also used extensively. Our use of this method traces back to the presentation by Chen [26], in which the method, known as Burg’s method, was applied to the extraction of spectral energy densities from seismic nonlinear time series

data. Chen [26] presented the first source code for the improvement of Burg's method in the extraction of the desired spectral information from the data.

One of the significant advantages of the maximum entropy method over the use of the filtered fast Fourier transform (FFT) method is the enhancement of the spectral peaks in the spectral energy density distribution. Our previous experience with the maximum entropy method and the existence of useful source codes for the analysis of the predicted time series led to our use of this method for the evaluation of the spectral entropy for each segment in the series of segments representing the complete nonlinear time series data. We refer interested readers to References [21–25] for information concerning acquisition of the various software and computer resources.

The method of analysis used for our study is the prediction of the distribution of the spectral entropy of the computed nonlinear time series. The individual fluctuating histories for the vertical and transverse velocity components are combined into one time series by adding the squares of each component for each time step. The total time series is divided into 768 segments with 32 data sets per segment. The maximum entropy method, (Press, *et al.* [25]), is then applied to each segment of 32 data sets to obtain 16 spiked values of the power spectral density, f_r , for each particular segment. The probability values of each set of particular spectral densities for each segment is then computed from $P_r = f_r / \sum_r f_r$. The methods of Powell and Percival [27], Grassberger and Procaccia [28], and Cohen and Procaccia [29] are then applied to the probability distributions for each segment to develop the spectral entropy for the given segment. The spectral entropy (dimensionless) is defined as:

$$s_{j_spent} = -\sum_r P_r \ln P_r \quad (15)$$

for the j-th segment. This procedure is applied to each of the 768 segments over the total time range.

To determine the over-all predicted spectral entropy change across the expansion, it is necessary to introduce the *activation spectral entropy* for each of the area ratios computed. The simple method of taking the overall average of the spectral entropy across the range of time steps and denoting this as the base spectral entropy, s_{1_spent} , and then taking the average of all spectral entropy values, denoted by s_{2_spent} , above the activation spectral entropy, yields the predicted change in dimensionless spectral entropy across the expansion as:

$$\Delta S_spent = (s_{2_spent}) - (s_{1_spent}). \quad (16)$$

To bring this computed value for the increase in spectral entropy across the expansion into agreement with the experimentally inferred value for the entropy increase requires the incorporation of precise values for the threshold spectral entropy above which the average is to be taken. If the threshold spectral entropy is too high, then only high values of spectral entropy will be included in the average and the overall predicted spectral entropy change is too high. If the threshold value for the spectral entropy is too low, then low values of spectral entropy are included in the average, and the predicted change is too low. By the *ad hoc* selection of these threshold values for the spectral entropy in the averaging process, the predicted increase in spectral entropy across the sudden expansion is brought into close agreement with the inferred entropy increase for the expansion as a function of area ratio.

3. Results and Discussion

The results for the integration of the equations for the wave numbers represent the conservation of mass in the overall set of equations. Figure 2 presents the perturbation factor F_1 as a function of time step through the first portion the overall time range. These results show the periodic behavior for the forcing function. Note that this forcing function is internal to the set of six equations describing the overall flow, but represent an externally applied forcing function for the three equations describing the equations of motion.

Figure 2. The periodic internal driving force obtained from the solution for the wave vectors from the continuity equations for an area ratio $A_1/A_2 = 0.30$.

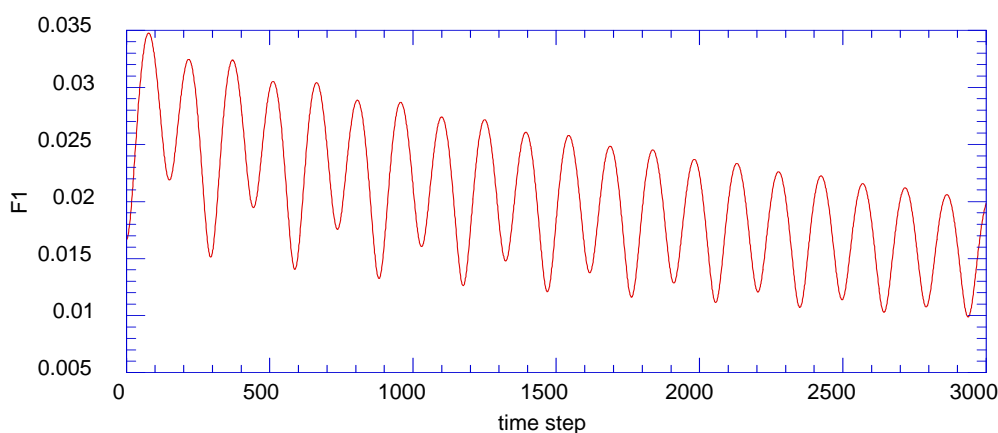


Figure 3 indicates the behavior of the vertical velocity component, a_y , with a moderate aperiodic behavior in the first part of the time series, with a transition to significant oscillations in the next part of the time series.

Figure 3. The vertical component of the fluctuating velocity a_y , as a function of the time step for an area ratio $A_1/A_2 = 0.30$.

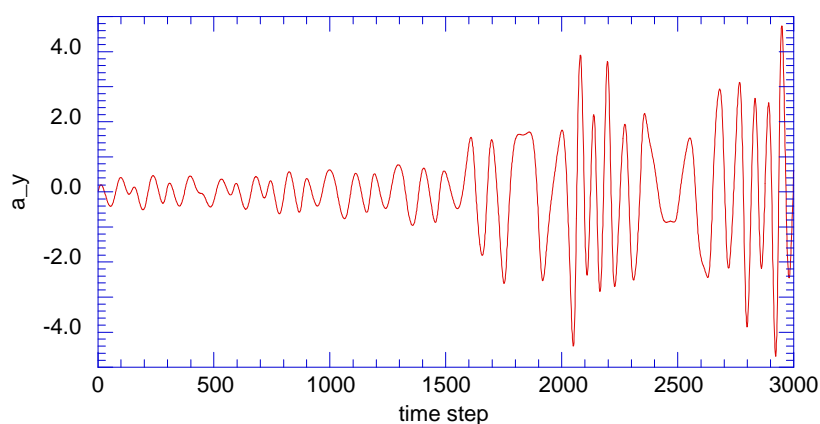
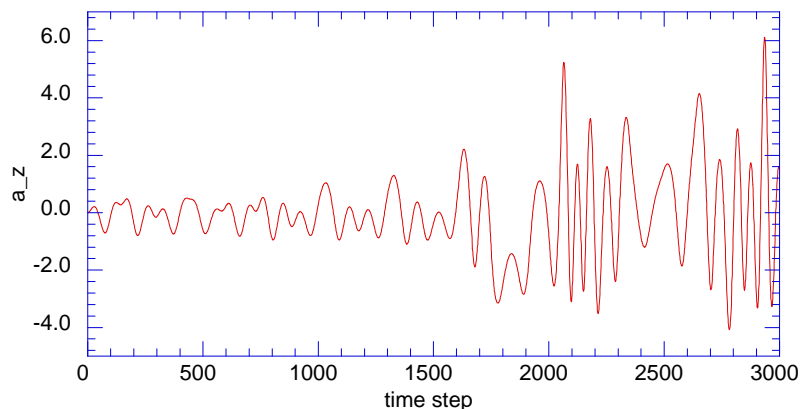


Figure 4 presents the time series for the span-wise component, a_z , which also represents this type of behavior. The span-wise fluctuating velocity component also indicates a transition to a significant level of oscillations, thus indicating the possible creation of ordered structures in the y-z plane in this region of the time series.

Figure 4. The span-wise component of the fluctuating velocity a_z as a function of the time step for an area ratio $A_1/A_2 = 0.30$.



It is interesting to note that Prichard and Theiler [30], in a study of the behavior of the Rössler attractor, observed that the local entropy is apparently large when the particular parameter is large. We, however, find that the spectral entropy is dependent on the degree of order within the flow element, with lower values of the spectral entropy representing a higher degree of order within the element. The spectral entropy does not seem to be dependent on the magnitude of the respective fluctuating velocity components, but rather increases as the degree of disorder increases.

Figure 5 presents the phase plane plot of the vertical component of velocity, a_y , versus the axial velocity component, a_x , over the initial time frame of 1,000 time steps. The portion of the results on the right-hand side of the figure represents a Duffing-like equation behavior (Lynch [31]), indicating a close coupling between the axial velocity component and the vertical velocity component. Then, the vertical velocity component accelerates to a constant velocity, as the axial velocity component decrease. This would indicate an almost organized motion of the system in the vertical direction.

Figure 5. The phase plane representation of the vertical fluctuating velocity a_y against the horizontal fluctuating velocity a_x over 1,000 time steps for an area ratio $A_1/A_2 = 0.30$.

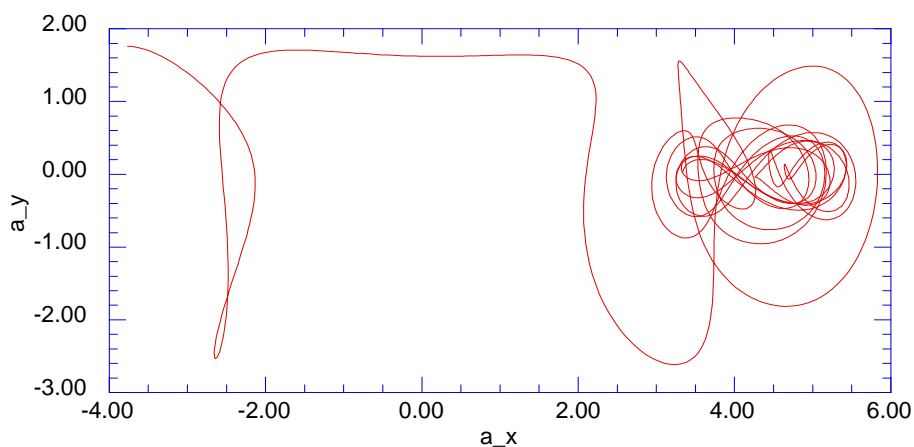
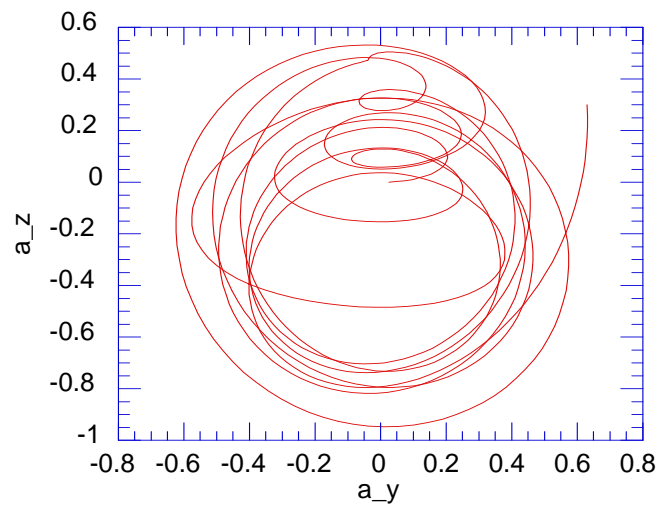


Figure 6 presents the phase plane results for the span-wise velocity component, a_z , versus the vertical velocity component, a_y , which indicates a nearly periodic rotational behavior in the vertical and span-wise plane.

Figure 6. The phase plane representation of the span-wise velocity fluctuations a_z against the vertical velocity fluctuations a_y over 1,000 time steps for an area ratio $A_1/A_2 = 0.30$.



During a previous study of the behavior of an internal free shear layer within a flow cavity in a subsonic wind tunnel (Isaacson [13]), a number of photographs of the flow structures along the shear layer were obtained. The flow conditions were not reported.

Figure 7 shows vertical flow structures in the physical domain that perhaps indicate an ordered value for the fluctuating vertical velocity. Note that Figure 5 presents results obtained from the Fourier analysis of the shear layer equations that indicate a nearly constant fluctuating vertical velocity across a significant time frame of the integration. Figure 8 presents a close-up of the first flow structure shown in Figure 7. Figure 8 indicates a possible vortex tube-type structure, inclined to the vertical span-wise plane. Again, the Fourier analysis results presented in Figure 6 indicate a periodic behavior for the a_z versus a_y phase plane. However, the physical flow structures shown in Figures 7 and 8 cannot be deduced from the fluctuating wave results presented in Figures 5 and 6.

Figure 7. The flow is from right to left across the sharp edge lower baffle of an internal cavity. The flow conditions were not reported.



Figure 8. An expanded view of the forward structure shown in Figure 7. The leftward slant of the structure may be due to the axial velocity of the mainstream flow.



As the time step continues, the fluctuation in the axial velocity component reaches a negative value, causing a transition of the vertical velocity component to a significantly larger fluctuation in value (Figure 9). It appears that as the fluctuating vertical and span-wise velocity components reach the region of increasing negative axial fluctuating velocity values, the system has reached a transition region, where the flow undergoes a significant change in behavior. Beyond this transition region, all three components of the flow velocity show large fluctuations in value (Figure 10).

Figure 9. The phase plane representation of the vertical velocity a_y versus the horizontal velocity a_x over 3,000 time steps for an area ratio $A_1/A_2 = 0.30$.

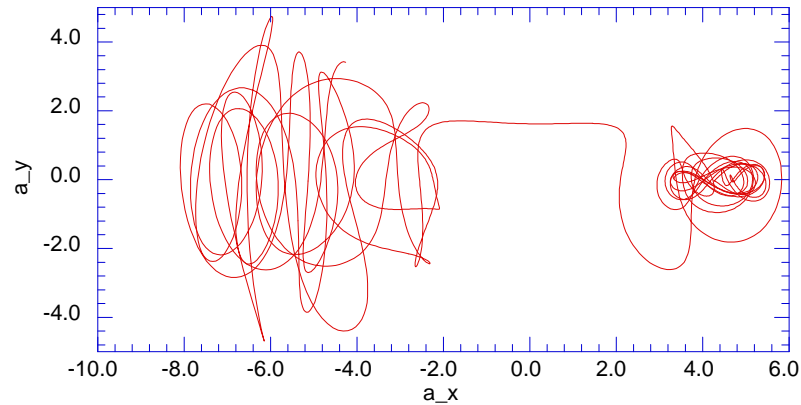
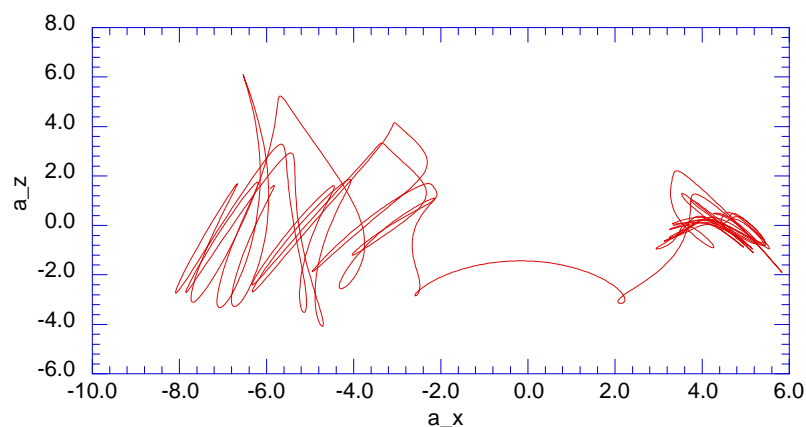


Figure 10. The phase plane representation of the span-wise velocity a_z versus the horizontal velocity a_x over 3,000 time steps for an area ratio $A_1/A_2 = 0.30$.



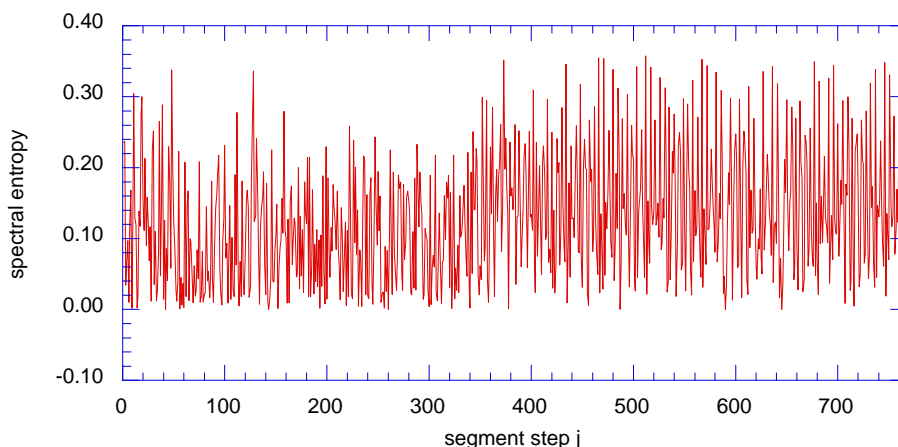
To obtain a numerical representation of this complex flow behavior, concepts from information theory as developed by Tribus [32] are applied. From the basic formalism of information theory as developed by Jaynes [7], Tribus expresses first the maximum of the entropy as described by the expression, $S_x = -\sum_i p_i \ln p_i$, where p_i represents the probability of finding the system in a given state i . Second, a Lagrangian multiplier is applied to the reality condition, $\sum_i dp_i = 0$. Finally, a second Lagrangian multiplier is applied to the conservation of overall energy of the system, $\sum_i \varepsilon_i dp_i = 0$. Application of the formalism presented by Tribus [32] leads to the distribution function for p_i in terms of a single Lagrangian multiplier, β , specified as the “temper” of the expected value of the energy of the system. The connection between the microscopic distribution function and the macroscopic concepts of thermodynamics is then made through an evaluation of the “pressure” of an ideal gas against the walls of the container of the system. Experimental comparison of the behavior of the “pressure” of the gas with the ideal gas equation yields the final result that $\beta = \frac{1}{kT}$, where k is Boltzmann’s constant and T is the temperature of the system. More general considerations yield the result that thermal equilibrium between systems defines the equality of the “temperature” of the systems. The essential point is that recourse must be made to experimental observations to bring the concepts of information theory to agreement with macroscopic thermodynamics.

To establish a similar form for the set of equations describing the flow through a sudden expansion, we employed the following procedure: First, the physics of the internal shear layer were represented in the form of six first-order differential equations. The first three equations represent the conservation of mass through the system. Second, the integration of the equations of motion and the computation of the kinetic energy associated with the vertical and span-wise velocity fluctuations were computed. Third, local spectral entropy was computed for regions across the entire time span of the computation. Figure 11 indicates that during the first of the time steps, the spectral entropy decreases, indicating an increase in information within the flow structures. The spectral entropy then increases over a relatively short time span as the flow transitions to the next region. In this region, the spectral entropy again decreases, again indicating an increase in the information content within the flow in that region. As the time steps continue, the flow transitions to the significant aperiodic behavior indicated in the remainder of Figure 11.

This region of spectral entropy values contributes to the predicted spectral entropy of the overall flow into the sudden expansion. Note that these values of the spectral entropy occur when the fluctuating axial velocity is in the negative range and produces the most vigorous part of the aperiodic motion. Prichard and Theiler [30] indicate that the most energetic of the fluctuating components of velocity will contribute to the spectral entropy through this region and that they will be subjected to the folding and stretching of the flow elements as they lose information to spectral entropy. This region is thus a region of “dissolution” where the incoming low spectral entropy flow is transformed into a high spectral entropy region. This region thus provides a flow reservoir of high spectral entropy elements which, through a “scrambling” process, reach the level of physical scales that ultimately dissipate into background thermodynamic entropy. Mathieu and Scott [33] have discussed this “scrambling” process

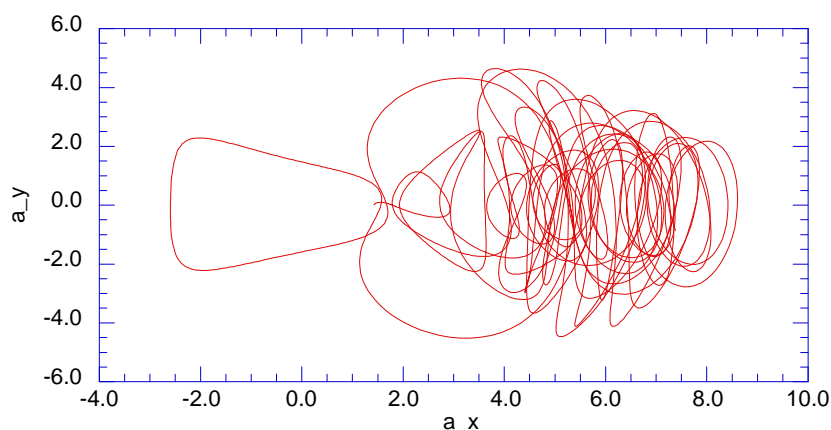
in much more detail. Sagaut and Camdon [34] have described the flow of high spectral entropy elements into the dissipation region as a “streaming” process.

Figure 11. Spectral entropy results for the fluctuating a_y and a_z velocity components by the maximum entropy method. $A_1/A_2 = 0.30$.



It is interesting to note that for the area ratios which produce the lowest inlet velocities, the results for the a_y versus a_x phase plane indicate weak oscillations primarily in the positive a_x region. As the flow inlet velocity is increased, the flow oscillations in the positive a_x region become stronger. For an area ratio of $A_1/A_2 = 0.70$, Figure 12 presents the phase plane representation of the vertical velocity component a_y versus the axial velocity component a_x for 3,000 time steps. The vertical fluctuations for this case also show a transition region toward the negative a_x region. However, these results indicate that the fluctuating vertical velocity component returns to the region of positive axial velocity fluctuations in a more orderly oscillation pattern.

Figure 12. The phase plane representation of the a_y fluctuating velocity component versus the a_x fluctuating velocity component for a count of 3,000 time steps for an area ratio $A_1/A_2 = 0.70$.

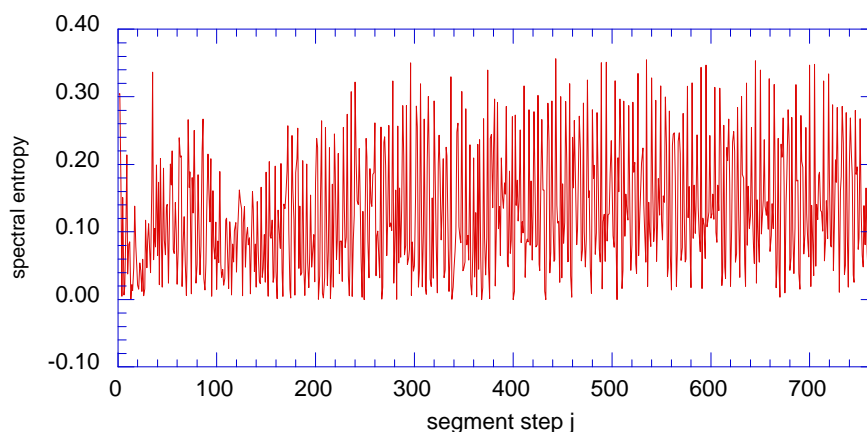


The spectral entropy results for the area ratio $\frac{A_1}{A_2} = 0.70$ are presented in Figure 13 and cover the entire time step range. Although these results appear to be similar to the results presented in Figure 11,

it must be noted that the flow behavior is different. The initial fluctuating vertical velocities occur again in the positive fluctuating axial velocity range. Then, the fluctuating vertical velocities again transition toward the negative axial velocity region. However, instead of crossing into the negative axial velocity region, the fluctuating vertical velocity vectors return to the positive fluctuating axial velocity vector region. Hence, the results for the low inlet axial velocity indicate a different behavior with considerably reduced average spectral entropy content. These results imply the existence of a transition region in the flow as the inlet flow velocity is increased from the initial low values to the higher values.

Even though the maximum spectral entropy values for the case of area ratio $A_1/A_2 = 0.70$ in Figure 13 are similar to those for the area ratio of $A_1/A_2 = 0.30$, it becomes necessary to take a much lower value of the spectral entropy threshold, or activation spectral entropy, to provide a predicted value of spectral entropy increase to correspond with the experimentally inferred value.

Figure 13. Spectral entropy results for the fluctuating a_y and a_z velocity components by the maximum entropy method for the area ratio $A_1/A_2 = 0.70$.

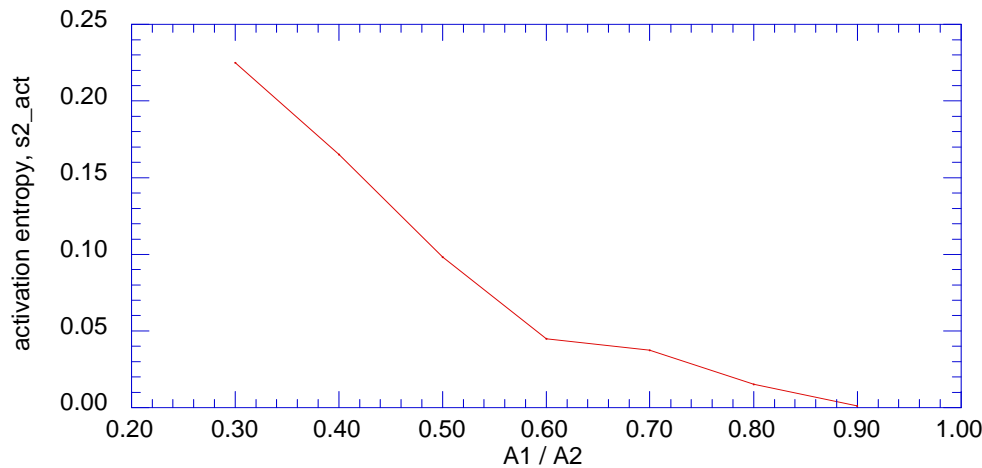


As the inlet flow velocity is increased to an area ratio $A_1/A_2 = 0.30$, the oscillations of the a_y component in the negative fluctuating axial velocity region are quite pronounced, with a significant spectral entropy produced. Thus, the activation spectral entropy values are strong functions of the inlet axial flow kinetic energy. It should be noted that once the entropy increase across the flow region has been determined, all other thermodynamic parameters could be determined by the methods of classical gas dynamics (Saad [35]).

The computed spectral entropy value across the expansion for each applied area ratio required the introduction of the threshold spectral entropy value. All of the spectral entropy values above the threshold were then averaged over the time step range to get the computed value to come into agreement with the inferred experimental entropy. The corresponding threshold spectral entropy values, or activation spectral entropies, are shown in Figure 14. The introduction of the activation spectral entropy above which the average of the spectral entropy values come into agreement with the experimentally-inferred values of overall entropy increase implies the existence of a potential barrier for the production of spectral entropy components which contribute to the overall irreversibility of the expansion process. Thus, thus, those more disordered structures which cross this threshold provide a

reservoir of such disordered structures, which then decay into structures of the scale that dissipate into background thermodynamic entropy.

Figure 14. Values of the *activation spectral entropy* as a function of the area ratio, A_1 / A_2 .



With the inclusion of the activation spectral entropy in the computations for the spectral entropy values across the range of expansion area ratios, the results for the computed spectral entropy values are brought into agreement with the implied measured entropy values.

3. Experimental Values for the Increase of Entropy

The experimental results for the loss of stagnation pressure across a dump combustor as measured by Barclay [8], and as correlated by Oates [9] serve as the benchmark against which we compare our theoretical predictions. The flow configurations that were used in the experimental project were circular ducts of different area ratios with abrupt expansions. The flow consisted of air and the flow was subsonic throughout. The inferred entropy changes across the expansion were obtained from the experimental results through the following analysis.

The Gibbs equation of thermodynamics may be written, in terms of stagnation properties, as:

$$T_t ds = dh_t - v_t dP_t. \quad (17)$$

In this equation, T_t is the stagnation temperature, s is the entropy, h_t is the stagnation enthalpy, v_t is the stagnation specific volume, and P_t is the stagnation pressure. For the adiabatic flow of an ideal gas, this may be integrated to the following expression, with R as the appropriate gas constant:

$$\frac{(s_2 - s_1)}{R} = -\ln\left(\frac{P_{t2}}{P_{t1}}\right). \quad (18)$$

Hence, given the experimental value for the decrease in stagnation pressure across the expansion, we may evaluate the experimental increase of entropy as:

$$\Delta S_{\text{exprmtl}} = \frac{s_2 - s_1}{R}. \quad (19)$$

This expression yields the dimensionless change in entropy for a given change in stagnation pressure from thermodynamic state 1 to thermodynamic state 2.

The series of experiments conducted by Barclay [8] yielded values for the loss in stagnation pressure across a “dump” combustor. The flow geometry consisted of a circular pipe of area A_1 with a sudden expansion into a downstream circular pipe of area A_2 , with the experiments conducted for a range of area ratios from

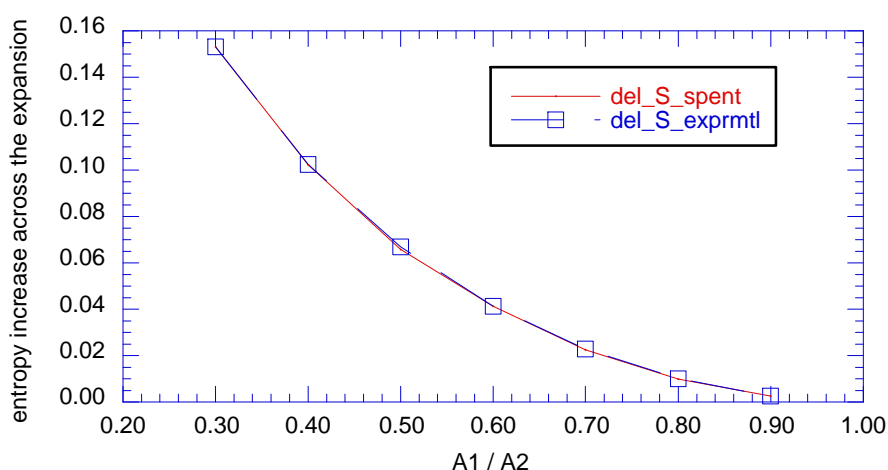
$$0.2 < A_1/A_2 < 1.0. \quad (20)$$

Oates [9] reports that the experimental results may be expressed as:

$$\frac{(s_2 - s_1)}{R} = \left\{ \left[1 - \left(\frac{A_1}{A_2} \right) \right]^2 + \left[1 - \left(\frac{A_1}{A_2} \right) \right]^6 \right\} \frac{\gamma}{2} M_1^2. \quad (21)$$

In this equation, γ is the ratio of specific heats and M_1 is the Mach number of the flow at area A_1 . This expression is used to obtain the dimensionless entropy increase across the sudden expansion for the range of area ratios $0.2 < A_1/A_2 < 1.0$. These results then serve as the test base against which the theoretical calculations are compared. The comparisons of the results are presented in Figure 15 and represent the overall results for this study.

Figure 15. Comparison of the computed spectral entropy increase with the experimental increase in entropy obtained from the measured loss of stagnation pressure as a function of the area ratio A_1/A_2 .



The introduction of the threshold spectral entropy, which we have called the *activation spectral entropy* is the *ad hoc* connection of the deterministic numerical predictions of the spectral entropy content with the experimentally inferred increase in entropy across the sudden expansion. We anticipate that future developments will provide a rational connection between the deterministic numerical results and the actual irreversible processes that occur in physical systems.

Table 1 presents the computed results for the increase of spectral entropy for each of the area ratios in the expansion process together with the inferred increase in entropy for the corresponding experimental area ratios. In Table 1, A_1/A_2 is the ratio of the inlet area to the exit area, s_1_spent is the overall average of the spectral entropy series, s_2_act is the activation spectral entropy, s_2_spent is the spectral entropy average above the activation spectral entropy, ΔS_spent is the predicted spectral entropy increase, and $\Delta S_exprmtl$ is the experimentally inferred value of the entropy increase.

Table 1. Summary of predicted entropy increases and corresponding experimentally inferred entropy values for the flow through a sudden expansion.

A_1/A_2	s_1_{spent}	s_2_{act}	s_2_{spent}	ΔS_{spent}	$\Delta S_{exprmtl}$
0.30	0.1271	0.2250	0.2802	0.1531	0.1531
0.40	0.1097	0.1650	0.2119	0.1022	0.1025
0.50	0.1255	0.0983	0.1913	0.0658	0.0669
0.60	0.0748	0.0450	0.1161	0.0413	0.0414
0.70	0.1303	0.0375	0.1529	0.0226	0.0229
0.80	0.0929	0.0153	0.1029	0.0100	0.0101
0.90	0.1232	0.0012	0.1258	0.0026	0.0025

4. Conclusions

The complete set of equations for the fluctuating velocity wave vectors within the internal free-shear layer downstream of the separation point in a sudden expansion has been reduced to a set of equations similar to the Lorenz equations with the introduction of an internal feedback control parameter for the non-linear terms in the equations. The results of the computations indicate the development of, initially, a region with behavior similar to Duffing-like oscillations, a second region with organized vertical and span-wise components of flow, and a region of complete transition into large fluctuating components. It should be noted that the computed values for the spectral entropy for each of the given area ratios is the spectral entropy of the squared values of the fluctuating vertical and span-wise velocity components at the peak of their aperiodic trajectories. The flow behavior then undergoes a “streaming” or a “dissolution” into the range of ultimate dissipation of the turbulent kinetic energy into background thermodynamic entropy. The results for the numerical calculations of spectral entropy increase across the sudden expansion are brought into agreement with the experimentally inferred entropy increase by the *ad hoc* introduction of a threshold spectral entropy value, which we have designated the *activation spectral entropy*.

Acknowledgements

The author would like to thank the editor and referees for their timely and helpful suggestions. Incorporation of these suggestions has significantly strengthened the presentation.

References

1. Gosman, A.D.; Pun, W.M.; Runchal, A.K.; Spalding, D.B.; Wolfshtein, M. *Heat and Mass Transfer in Recirculating Flows*; Academic: London, UK, 1969.
2. Patankar, S.V. *Numerical Heat Transfer and Fluid Flow*; Hemisphere: New York, NY, USA, 1980.
3. Pantankar, S.V. *Computation of Conduction and Duct Flow Heat Transfer*; Innovative Research: Maple Grove, MN, USA, 1991.
4. Hirsch, C. *Numerical Computation of Internal and External Flows: Fundamentals of Computational Fluid Dynamics*; Butterworth-Heinemann: Burlington, MA, USA, 2007.
5. Abu-Nada, E. Numerical prediction of entropy generation in separated flows. *Entropy* **2005**, *4*, 234–252.

6. Yapici, H.; Kayatas, N.; Kahraman, N.; Basturk, G. Numerical study on local entropy generation in compressible flow through a suddenly expanding pipe. *Entropy* **2005**, *7*, 38–67.
7. Jaynes, E.T. Information theory and statistical mechanics. II. *Phys. Rev.* **1957**, *108*, 171–190.
8. Barclay, L.P. AF Aero Propulsion Laboratory: Wright-Patterson AFB, OH, USA. Pressure losses in dump combustors, unpublished work, 1972.
9. Oates, G.C. *Aerothermodynamics of Gas Turbines and Rocket Propulsion*; AIAA: Washington, DC, USA, 1988; pp. 60–61.
10. Landau, L.D.; Lifshitz, E.M. *Quantum Mechanics: Non-Relativistic Theory*; Pergamon Press, Ltd.: London, UK, 1958; pp. 133–144.
11. Townsend, A.A. *The Structure of Turbulent Shear Flow: Second Edition*; Cambridge University Press: Cambridge, UK, 1976, pp. 45–49.
12. Hellberg, C.S.; Orszag, S.A. Chaotic behavior of interacting elliptical instability modes. *Phys. Fluid.* **1988**, *31*, 6–8.
13. Isaacson, L.K. A deterministic prediction of ordered structures in an internal free shear layer. *J. Non-Equilib. Thermodyn.* **1993**, *18*, 256–270.
14. Pyragas, K. Continuous control of chaos by self-controlling feedback. *Phys. Lett. A* **1990**, *170*, 421–427.
15. Pyragas, K. Predictable chaos in slightly perturbed unpredictable chaotic systems. *Phys. Lett. A* **1993**, *181*, 203–210.
16. Glasstone, S.; Laidler, K.J.; Eyring, H. *The Theory of Rate Processes*; McGraw-Hill Book Company, Inc.: New York, NY, USA, 1941; pp. 21–27.
17. Stuart, J.T. On finite amplitude oscillation in laminar mixing layers. *J. Fluid Mech.* **1967**, *29*, 417.
18. Kirchoff, R.H. *Potential Flows: Computer Graphics Solutions*; Marcell Dekker, Inc.: New York, NY, USA 1985; p. 71.
19. Press, W.; Teukilsky, S.A.; Vetterling, W.T.; Flannery, B.P. *Numerical Recipes in C: The Art of Scientific Computing*, 2nd ed.; Cambridge University Press: Cambridge, UK, 1992; pp. 710–714.
20. Golyandina, N.; Nekrutkin, V.; Zhigljavsky, A. *Analysis of Time Series Structure: SSA and Related Techniques*; CRC Press LLC.: Boca Raton, FL, USA, 2001.
21. Hassani, H.; Heravi, S; Zhigljavsky, A. Forecasting European industrial production with singular spectrum analysis. *Int. J. Forecast.* **2009**, *25*, 103–118.
22. Press, W.; Teukilsky, S.A.; Vetterling, W.T.; Flannery, B.P. *Numerical Recipes in C: The Art of Scientific Computing*, 2nd ed.; Cambridge University Press: Cambridge, UK, 1992; pp. 676–688.
23. Kantz, H.; Schreiber, T. *Nonlinear Time Series Analysis*, 2nd ed.; Cambridge University Press: Cambridge, UK, 2004; pp. 154–173.
24. Maindonald, J.; Braun, W.J. *Data Analysis and Graphics Using R: An Example-Based Approach*, 3rd ed.; Cambridge University Press: Cambridge, UK, 2010.
25. Press, W.; Teukilsky, S.A.; Vetterling, W.T.; Flannery, B.P. *Numerical Recipes in C: The Art of Scientific Computing*, 2nd ed.; Cambridge University Press: Cambridge, UK, 1992; pp. 572–575.
26. Chen, C.H. *Digital Waveform Processing and Recognition*; CRC Press, Inc.: Boca Raton, FL, USA, 1982; pp. 131–158.
27. Powell, G.E.; Percival, I.C. A spectral entropy method for distinguishing regular and irregular motion for Hamiltonian systems. *J. Phys. Math. Gen.* **1979**, *12*, 2053–2071.

28. Grassberger, P.; Procaccia, I. Estimation of the Kolmogorov entropy from a chaotic signal. *Phys. Rev. A* **1983**, *28*, 2591–2593.
29. Cohen, A.; Procaccia, I. Computing the Kolmogorov entropy from time signals of dissipative and conservative dynamical systems. *Phys. Rev. A* **1985**, *31*, 1872–1882.
30. Prichard, D.; Theiler, J. Generalized redundancies for time series analysis. *Phys. Nonlinear Phenom.* **1995**, *84*, 476–493.
31. Lynch, S. *Dynamical Systems with Applications Using MATLAB*; Birkhauser: Boston, MA, USA, 2004; pp. 309–314.
32. Tribus, M. *Thermostatistics and Thermodynamics: An Introduction to Energy, Information and States of Matter, with Engineering Applications*; D. Van Nostrand Company, Inc.: Princeton, NJ, USA, 1961; pp. 75–86.
33. Mathieu, J.; Scott, J. *An Introduction to Turbulent Flow*; Cambridge University Press: Cambridge, UK, 2000; p. 299.
34. Sagaut, P.; Cambon, C. *Homogeneous Turbulence Dynamics*; Cambridge University Press: New York, NY, USA, 2008; p. 75.
35. Saad, M.A. *Compressible Fluid Flow*; Prentice-Hall, Inc.: Englewood Hills, NJ, USA, 1985; pp. 190–225.

© 2011 by the authors; licensee MDPI, Basel, Switzerland. This article is an open access article distributed under the terms and conditions of the Creative Commons Attribution license (<http://creativecommons.org/licenses/by/3.0/>).